Article

Numerical Study on the Heat Dissipation Performance of Diamond Microchannels under High Heat Flux Density

Jiwen Zhao [1], Kunlong Zhao [1], Xiaobin Hao [1,4], Yicun Li [2], Sen Zhang [1], Benjian Liu [1], Bing Dai [1], Wenxin Cao [2,*] and Jiaqi Zhu [1,2,3,*]

1. National Key Laboratory of Science and Technology on Advanced Composites in Special Environments, Harbin Institute of Technology, Harbin 150080, China
2. Zhengzhou Research Institute, Harbin Institute of Technology, Zhengzhou 450000, China
3. Key Laboratory of Micro-Systems and Micro-Structures Manufacturing, Ministry of Education, Harbin 150080, China
4. Henan Core-Diamond Material Technology Co., Ltd., Zhengzhou 450000, China
* Correspondence: caowenxin@hit.edu.cn (W.C.); zhujq@hit.edu.cn (J.Z.)

Abstract: Heat dissipation significantly limits semiconductor component performance improvement. Thermal management devices are pivotal for electronic chip heat dissipation, with the enhanced thermal conductivity of materials being crucial for their effectiveness. This study focuses on single-crystal diamond, renowned for its exceptional natural thermal conductivity, investigating diamond microchannels using finite element simulations. Initially, a validated mathematical model for microchannel flow heat transfer was established. Subsequently, the heat dissipation performance of typical microchannel materials was analyzed, highlighting the diamond's impact. This study also explores diamond microchannel topologies under high-power conditions, revealing unmatched advantages in ultra-high heat flux density dissipation. At 800 W/cm^2 and inlet flow rates of 0.4–1 m/s, diamond microchannels exhibit lower maximum temperatures compared to pure copper microchannels by 7.0, 7.2, 7.4, and 7.5 °C, respectively. Rectangular cross-section microchannels demonstrate superior heat dissipation, considering diamond processing costs. The exploration of angular structures with varying parameters shows significant temperature reductions with increasing complexity, such as a 2.4 °C drop at i = 4. The analysis of shape parameter k_i indicates optimal heat dissipation performance at k_i = 1.1. This research offers crucial insights for developing and optimizing diamond microchannel devices under ultra-high-heat-flux-density conditions, guiding future advancements in thermal management technology.

Keywords: diamond microchannels; heat dissipation; ultra-high thermal conductivity; high heat flux density; thermal management; semiconductor cooling

1. Introduction

Currently, the reliability of electronic components is significantly influenced by temperature. When the operating temperature of electronic components reaches 70–80 °C, for every 1 °C increase in temperature, their reliability decreases by 5% [1]. In fact, over 55% of electronic device failures are primarily caused by excessively high operating temperatures [2]. Taking silicon (Si)-based devices as an example, their maximum operating temperature is 175 °C. To ensure safe operation, the maximum operating temperature of civilian-grade chips should not exceed 70 °C, while industrial-grade chips are limited to 85 °C [3], and military-grade chips must remain below 128 °C. Excessive temperatures can lead to thermal failure in high-density integrated microsystems, emphasizing the critical importance of temperature control for electronic devices.

Liquid cooling refers to the use of a liquid coolant flowing through equipment for heat dissipation [4–6], which can effectively improve heat dissipation efficiency [7,8]. It

is widely used in high-performance computers, 5G base stations, and other high-heat-flux-density electronic component heat dissipation fields [9–12]. With the development of characterization and precision machining methods, scientists have begun to study the flow and heat dissipation behaviors of fluids at the micrometer scale [13,14]. Microchannel heat sink cooling technology was first proposed by Tuckerman and Pease [15] in 1981. Microchannel heat dissipation is an active heat dissipation method. However, there are currently two challenges in the field of microchannel chip heat dissipation: the inherent heat dissipation performance of the heat dissipation material, and the structure of the chip heat dissipation component. Heat dissipation materials with high thermal conductivity are beneficial for the overall heat dissipation of chips [16,17]; therefore, diamond and its composite materials, which have the highest thermal conductivity in nature, have attracted the attention of researchers. Out of all the naturally occurring materials, diamond exhibits the highest thermal conductivity, ranging from 1000 to 2200 W/(m·K) [18,19], and its thermal conductivity is more than five times that of copper, a commonly used heat dissipation material.

The ultra-high thermal conductivity of diamond makes it an ideal material for creating microchannels [20], particularly in applications with high heat flux density (>200 W/cm^2), where it offers unique advantages. With the advancement of microfluidic technology, scientists have begun to utilize diamond microchannels as efficient heat dissipation devices [21,22]. Yang et al. [22] selected diamond with a thermal conductivity of up to 1500 W/(m·K) as the material for microchannel heat sinks. They uniformly designed 37 parallel triangular microchannels with an aspect ratio of 5 on diamond films using laser ablation technology. The channels were 45 mm long with a hydraulic diameter of 280 μm. Diamond microchannels demonstrate exceptional heat dissipation performance under high-heat-flux-density conditions, maintaining a heat source temperature of 53.3 °C at a heat flux density of 267 W/cm^2. Tu et al. [23] investigated the durability of diamond microchannels in practical applications through surface modification techniques. They treated diamond microchannels with acid to achieve hydrophilic surfaces, followed by hydrogen and fluorine plasma etching to create hydrophobic walls. Decreasing the hydrophobicity of diamond microchannels increased the surface heat transfer coefficient by 11%.

Moreover, appropriate microchannel geometry can effectively harness the heat dissipation potential of microchannels [24]. The influence of microchannel shape on heat dissipation performance can be categorized into two aspects: the impact of microchannel cross-sectional shape on heat dissipation efficiency, and the influence of the overall microchannel path structure on heat dissipation effectiveness [25–27]. Deng et al. [28] compared five types of double-layer microchannel heat sinks with different cross-sectional shapes (triangular, rectangular, trapezoidal, circular, and folded Ω-shaped) and found that the double-layer microchannel heat sink with trapezoidal microchannels exhibited the poorest heat dissipation performance in terms of thermal resistance and pressure drop, while the double-layer microchannel heat sink with rectangular cross-sectional microchannels exhibited the best heat dissipation performance. Faraz Ahmad et al. [29] used ANSYS Fluent to analyze the heat dissipation performance of microchannel heat sinks with various geometric shapes (rectangular, circular, elliptical, trapezoidal, hexagonal, and irregular shapes with plus signs). They evaluated different channels based on criteria such as pressure drop, wall temperature, thermal enhancement factor, thermal resistance, heat transfer efficiency, and entropy generation rate. Overall, microchannels with irregular cross-sectional shapes and plus signs achieved the best performance across all metrics, followed by rectangular and trapezoidal shapes. Circular, elliptical, and hexagonal cross-sectional shapes exhibited the least effective heat dissipation performance in their study. Jing et al. [30] conducted a numerical analysis to study the thermodynamic properties of water flow in microchannels with three different cross-sectional shapes: rectangular, elliptical, and isosceles triangular. They applied two size constraints: one based on a constant microchannel cross-sectional area and the other on a constant microchannel circumference. Among the three cross-sectional shapes, triangular microchannels demonstrated the lowest hydraulic resistance

and convective heat transfer coefficient under various size constraints. However, for elliptical and rectangular microchannels, there exists a hydraulic diameter threshold that affects their hydraulic and thermal performance. When the hydraulic diameter of rectangular microchannels is below this threshold, they exhibit higher hydraulic resistance and convective heat transfer coefficients. Conversely, when the hydraulic diameter exceeds the threshold, elliptical microchannels show higher hydraulic resistance and convective heat transfer coefficients. Parlak [31] investigated the heat dissipation performance differences among three types of microchannels (straight channel, wavy channel, and serrated channel) using ANSYS. Their results indicated that within a Reynolds number (Re) range of 100–400, the Nusselt number of wavy channels was 10% higher than that of serrated channels and 40% higher than that of straight channels. Additionally, under inlet pressure conditions not exceeding 10 kPa for straight channels, the calculated inlet pressure data for serrated and wavy channels were nearly identical. Dai et al. [32] conducted experimental research on fluid dynamics and the heat dissipation performance of microchannels within the range of 50 < Re < 900. They found that compared to straight channels, wavy channels exhibited improved heat dissipation effects but also resulted in increased pressure drop. The flow recirculation and secondary flow induced by bends contributed to enhancing the heat dissipation efficiency of microchannels.

Currently, the application of diamond microchannels for high heat flux density heat dissipation is limited by material costs and processing technology, resulting in relatively few reports in this field. This study focuses on diamond microchannels to investigate their heat dissipation performance under high-heat-flux-density conditions (200–1200 W/cm^2), using inlet temperature and average pressure as key indicators. This research compares the heat dissipation performances of different microchannel matrix materials under ultra-high-heat-flux-density conditions. Additionally, it analyzes how the geometric structure of diamond microchannels influences their heat dissipation performance, proposing a multi-periodic diamond microchannel structure with an hourglass shape. This study explores the effects of the number of periods i and the shape parameter k_i on heat dissipation performance. This study establishes a foundational understanding of diamond microchannels under ultra-high-heat-flux-density conditions, offering significant practical implications for the high-power electronics industry.

2. Materials and Methods

2.1. Mathematical Model

The energy conservation equation [33] for the overall microchannel can be expressed as

$$\rho C_p \mathbf{u} \cdot \nabla T + \nabla \cdot \mathbf{q} = Q \tag{1}$$

where ρ denotes the density of the diamond substrate or coolant (kg/m^3), C_p denotes the specific heat capacity of the diamond substrate or coolant (J/(kg·°C), Q denotes the heat source, and **q** can be expressed as

$$\mathbf{q} = -k \nabla T \tag{2}$$

where k denotes the thermal conductivity of the diamond substrate or coolant (W/(m·K)).

The momentum and mass conservation equation of the coolant can be expressed as

$$\rho(\mathbf{u} \cdot \nabla)\mathbf{u} = \nabla \cdot [-p\mathbf{I} + \mathbf{K}] + \mathbf{F} \tag{3}$$

$$\nabla \cdot \mathbf{u} = 0 \tag{4}$$

where **u** denotes the flow velocity of the coolant (m/s), p denotes the pressure of the coolant (Pa), **I** denotes the second-order unit tensor, **F** denotes the volumetric force exerted on the coolant as a whole (N), and **K** denotes the viscous stress tensor. K can be calculated using the following equation:

$$\mathbf{K} = \mu\left(\nabla \mathbf{u} + (\nabla \mathbf{u})^\top\right) \tag{5}$$

where μ denotes the dynamic viscosity of the coolant (mPa·s).

It is important to note the presence of interface thermal resistance between gallium nitride material (GaN) and diamond. This article employs an equivalent thin thermal resistance layer, calculated using the following formulas:

$$-\mathbf{n}_{\text{GaN}} \cdot \mathbf{q}_{\text{GaN}} = -h_{\text{eq}}(T_{\text{Dia}} - T_{\text{GaN}}) \tag{6}$$

$$-\mathbf{n}_{\text{Dia}} \cdot \mathbf{q}_{\text{Dia}} = -h_{\text{eq}}(T_{\text{GaN}} - T_{\text{Dia}}) \tag{7}$$

where $\mathbf{n}_{\text{GaN}}$ and $\mathbf{n}_{\text{Dia}}$ denote the normal unit vectors of the contact surface between diamond and GaN, T_{Dia} denotes the temperature of the diamond layer (°C), T_{GaN} represents the temperature of the GaN layer (°C), and h_{eq} denotes the equivalent interfacial thermal conductivity (W/(m²·K)), which can be expressed as

$$h_{\text{eq}} = \frac{1}{R_{\text{eq}}} \tag{8}$$

where R_{eq} denotes the equivalent thermal resistance value (m²·K/W). In practical applications, to ensure bonding strength between GaN and diamond, a layer of silicon nitride material (SiN) is typically interposed between them. The thermal resistance between GaN and diamond primarily arises from two sources: (1) the volumetric thermal resistance of the SiN layer, and (2) the thermal resistances at the interfaces of GaN/SiN and SiN/diamond. The existing literature suggests that the equivalent thermal resistance between GaN and diamond generally falls within the range of $6.5 - 50 \times 10^{-9}$ m² K/W [34–36], while the the R_{eq} value in this study was 30×10^{-9} m² K/W [37].

2.2. Numerical Model and Boundary Condition

2.2.1. Geometric Model Settings

We established the model based on the commercial software COMSOL 6.2 [14]. The boundary conditions of the model are illustrated in Figure 1, depicting a GaN layer of thickness H_1 on top. A surface heat source with a heat flux density q is positioned above the GaN. The bottom surface of the diamond features an open boundary with a heat transfer coefficient of h_0. An interface thermal resistance is specified between the GaN and diamond layers. For ease of grid partitioning, a plane is positioned 1 mm away from the GaN–diamond interface in this study. The microchannel inlet velocity is denoted as U_0, with microchannel width L_f, spacing between microchannels δ, and microchannel height H_f. The bottom surface acts as an open boundary for natural convection, with a heat flux corresponding to natural air dissipation (20 W/(m²·K)). Other sidewalls are assumed to be insulated, neglecting heat dissipation from these surfaces.
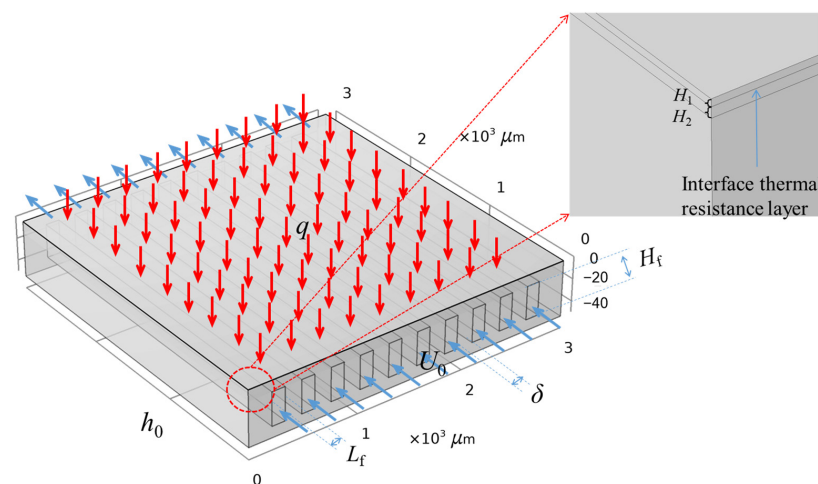

Figure 1. Boundary conditions set in the model.

The solid part of the microchannel heat dissipation model is primarily divided into GaN, the solid material of the microchannel, and the liquid material. The thermal conductivity of GaN varies with temperature and thickness. This study utilizes thermal conductivity data from Song et al. [37], as shown in Table 1.

Table 1. Interpolation of GaN thermal conductivity.

Temperature (K)	200	250	300	350	400	450	500	550	600
0.7 μm (W/(m·K))	136	120	107	96	88	81	74	69	65

The other physical parameters are listed in Table 2.

Table 2. Comparison of physical properties of typical microchannel coolants.

	Material	Density (Kg/m^3)	Specific Heat Capacity (J/(kg·K))	Thermal Conductivity (W/(m·K))	Dynamic Viscosity (mPa·s)
	GaN		6150	670	
	Diamond	3512	510	1800	–
	Silicon	2230	712	148	–
Solid	Copper	8920	390	400	–
	LTCC	2500	900	3	–
	Aluminum	2702	880	237	–
Liquid	Deionized water	1000	4200	0.61	1

Table 3 lists the geometric parameter values of the microchannel model.

Table 3. Geometric parameters of microchannels.

Parameter	Value	Meaning
L	3 mm	Horizontal length
W	3 mm	Horizontal width
H_1	0.7 μm	GaN thickness
H_2	1 μm	
L_f	120 μm	Width of microchannels
δ	150 μm	Microchannel spacing
H_f	300 μm	Microchannel height

2.2.2. Grid Independence Analysis

The grid division consists of three main parts. The first part encompasses the GaN layer and diamond region up to height H_2 in Figure 1. The horizontal grid is structured into a free quadrilateral grid, which is then swept vertically. The GaN layer includes 2 scanning layers, and the H_2 layer includes 3 scanning layers. The second part covers the diamond region excluding H_2, which is meshed using a free tetrahedral mesh. The third part involves the microchannel region, divided into free tetrahedral grids, as shown in Figure 2.
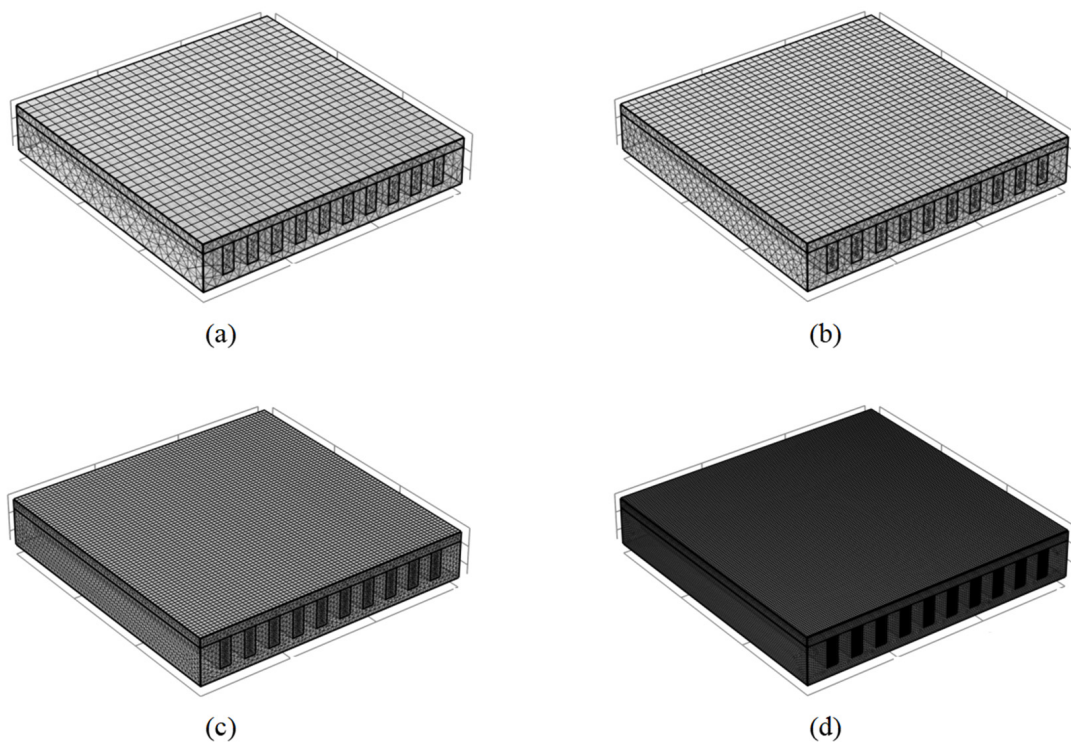
The simulation results obtained from coarse grids show significant errors, whereas excessively dense grids can decrease the computational efficiency of the model. To strike a balance between numerical accuracy and computational costs, we conducted a grid independence test. Following the grid partitioning principles outlined above, this section presents the calculation results for four different grid densities (partitioning criteria are detailed in Table 4, and partitioning results are illustrated in Figure 3).
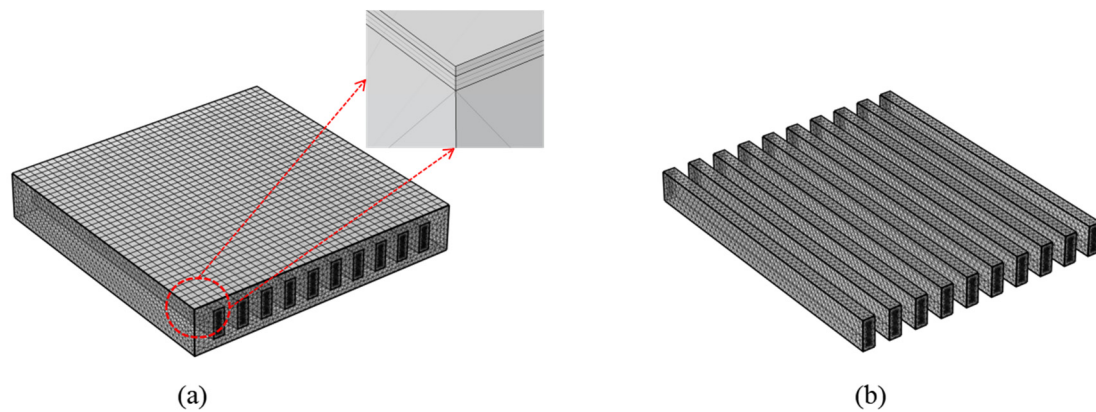
Figure 2. Grid division: (**a**) overall grid division and (**b**) microchannel region grid division.

Table 4. Grid partitioning schemes with varying densities.

Grid Division	Part 1. Maximum Unit Size/(μm)	Part 2. Maximum Unit Size (μm)	Part 3. Maximum Unit Size (μm)
Plan A	160	120	20
Plan B	80	60	10
Plan C	40	30	5
Plan D	20	15	2

Figure 3. Grid division with different densities: (**a**) Plan A, (**b**) Plan B, (**c**) Plan C, and (**d**) Plan D.

This section employs a heat source surface density of 800 W/cm² and an inlet flow velocity of 1 m/s. Table 5 displays the highest temperatures calculated under various grid densities.

From Table 5, it can be observed that there is no significant difference in the calculation results when using Plan B. To reduce computational complexity while maintaining accuracy, the grid partitioning strategy proposed in Plan B was adopted for subsequent calculations.

Table 5. Maximum temperature of chips under various grid partitioning methods.

Grid Division	Plan A	Plan B	Plan C	Plan D
Maximum temperature (°C)	90.4 °C	88.34 °C	88.32 °C	88.32 °C

2.2.3. Validation

Further comparative verification was conducted using the calculation case described in reference [38]. The microchannel structure is depicted in Figure 4a, and the temperature distribution along the channel is illustrated in Figure 4b. Here, the horizontal axis represents the position distribution along the channel direction (from inlet to outlet), while the vertical axis represents the average temperature of the channel wall at position x [38]. We adopted the same material properties and geometric parameters as in the literature (α = 8°, ε = 8, L = 20 mm, H = 80 μm), set the bottom heat flux density of the microchannel to 20,000 W/m^2, and set the fluid Reynolds number to 200. Under identical calculation conditions, the temperature distribution results within the flow channel in this model align well with experimental data from the literature, validating the reasonableness of the computational approach adopted in this section.

(a)　　　　　　　　　　　　　　　　(b)
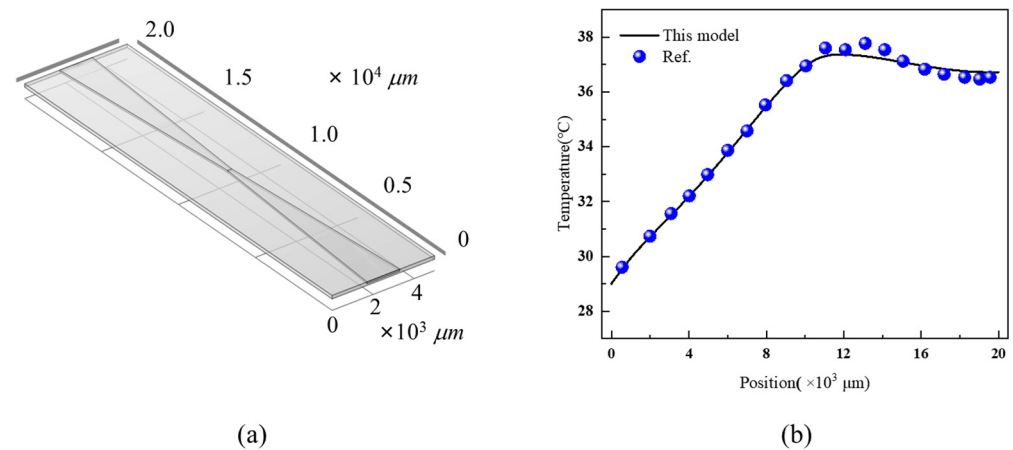
Figure 4. Calculation model validation: (**a**) geometric structure of microchannels; (**b**) comparison of experimental and simulated average wall temperatures along the channel direction (normal direction from the inlet to the outlet) [38].

3. Results and Discussion

*3.1. The Influence of Material Physical Properties on the Heat Dissipation Performance of Microchannels*

3.1.1. Comparison of Heat Dissipation Performance of Different Microchannel Materials

This section analyzes the heat dissipation performance of microchannels with various substrate materials and examines the variation in the highest temperature of the GaN layer under different flow rates and heat flux densities, as depicted in Figure 5.

Compared with other substrate materials, low-temperature cofired ceramic (LTCC) has a lower thermal conductivity, resulting in significantly higher chip temperatures under identical conditions. Even at a heat flux density of 200 W/cm^2 and a flow rate of 1.2 m/s, the maximum temperature of the chip exceeds the upper limit of GaN chip operating temperatures, making LTCC unsuitable for dissipating heat in chips with high heat flux densities. This section compares the highest temperatures of four typical flow velocities (0.4 m/s, 0.6 m/s, 0.8 m/s, 1.0 m/s) across different substrate materials at varying heat flux densities, illustrated in Figure 6.

It is evident that as the heat flux density increases, the superior heat dissipation performance of diamond microchannels becomes increasingly pronounced. At a heat flux density of 800 W/cm^2 and inlet flow rates of 0.4, 0.6, 0.8, and 1 m/s, the maximum temperature of diamond microchannels is lower than that of pure copper microchannels by

7.0 °C, 7.2 °C, 7.4 °C, and 7.5 °C, respectively. The difference in the maximum temperature between diamond and pure copper microchannels shows a gradual increase with higher flow rates. This underscores the critical role of diamond microchannels in high-heat-flux-density-heat-dissipation applications, emphasizing the importance of considering cooling liquid flow rates to ensure chips operate within their designated temperature ranges for specific practical applications.
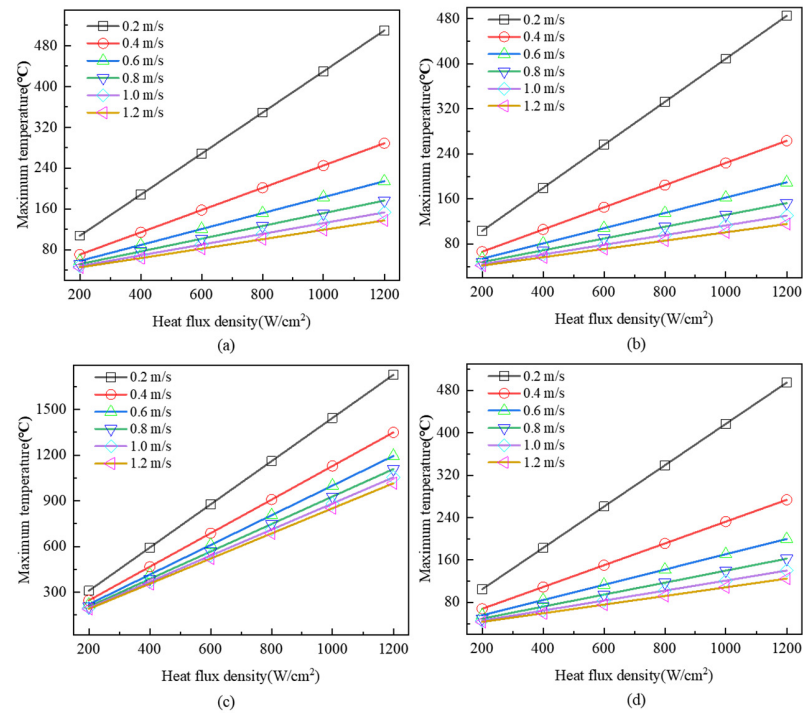
Figure 5. Relationship between maximum temperature and heat flux density of microchannels under different flow rate conditions: (**a**) silicon, (**b**) copper, (**c**) LTCC, and (**d**) aluminum.
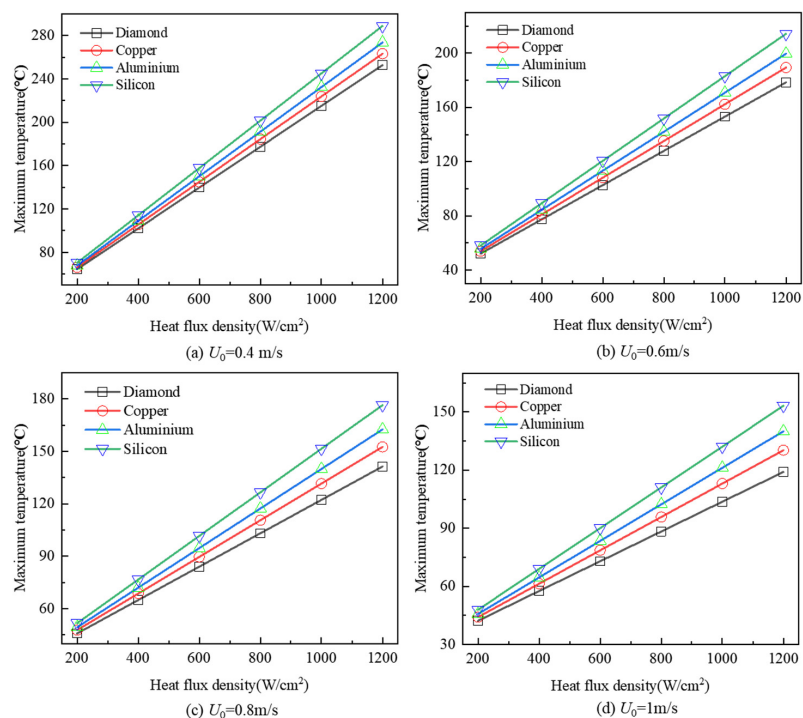
Figure 6. Comparison of maximum temperatures of different substrate materials at various heat flux densities.

3.1.2. Exploration of Diamond Thermal Conductivity on Microchannel Heat Dissipation Performance

This section further investigates the superior heat dissipation performance of diamond under high-power conditions. Given that the thermal conductivity of diamond typically ranges from 1000 to 2200 W/(m·K) in practical applications, this study examined several typical values (1200, 1500, 2100 W/(m·K)) to assess how variations in diamond thermal conductivity affect microchannel heat dissipation performance.

In observing Figure 7, it is evident that increasing thermal conductivity has a moderate impact on the overall heat dissipation performance. At a heat flux density of 800 W/(m·K) and an inlet flow rate of 1 m/s, the highest temperature decreases with increasing diamond thermal conductivity. The highest temperatures under the four thermal conductivity conditions were 89.3 °C, 88.7 °C, 88.3 °C, and 88.0 °C, respectively. It is clear that higher thermal conductivity improves the heat dissipation performance of diamond microchannels to a certain extent. However, beyond a thermal conductivity of 1800 W/(m·K), the enhancement in heat dissipation performance diminishes. This suggests that while high substrate thermal conductivity is crucial for improving microchannel heat dissipation, the cost-effectiveness decreases significantly once thermal conductivity exceeds 1800 W/(m·K).
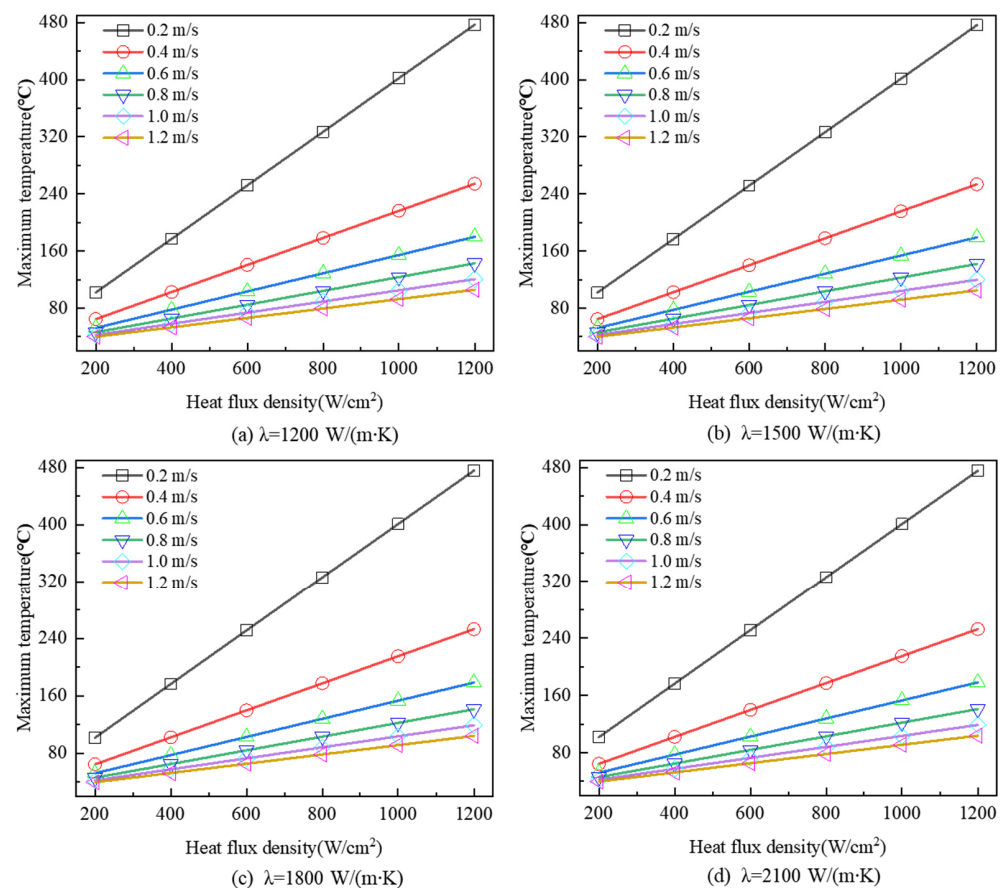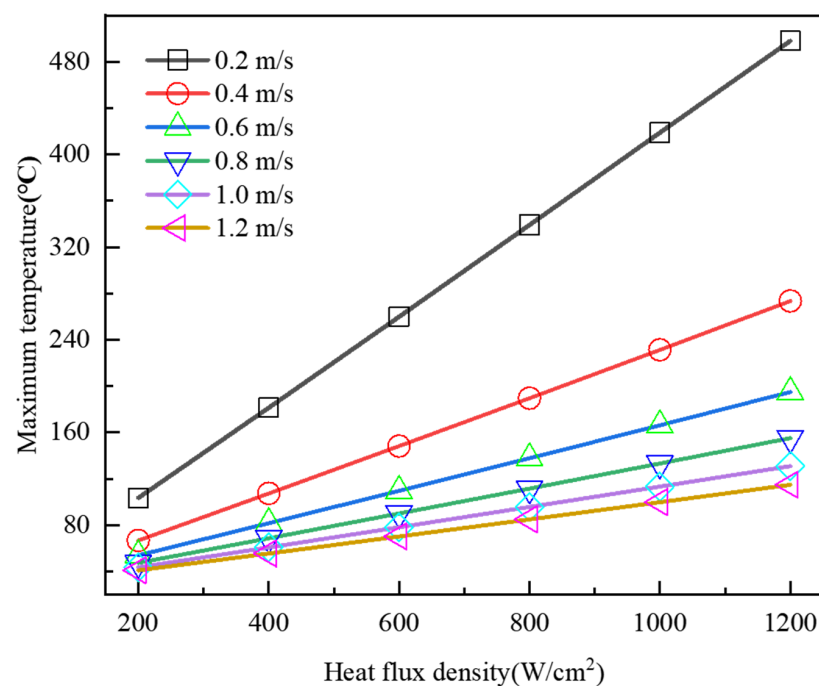

Figure 7. Comparison of heat dissipation performance of diamonds with different thermal conductivities.

However, studies indicate that diamond exhibits varying thermal conductivities along its thickness owing to its growth characteristics, notably its columnar growth pattern. This variation results in significantly increased thermal conductivity with increasing thickness [18]. Considering this, Table 6 presents the thermal conductivity of diamond at different thicknesses and temperatures [37]. For thickness exceeding 100 μm, this section approximates the thermal conductivity of diamond within the range of 35–100 μm. The calculation results of the heat dissipation effect of diamond microchannels at different flow rates are shown in Figure 8.

Table 6. Thermal conductivity of diamond at various thicknesses and temperatures.

Temperature (K)	0–1 μm (W/(m·K))	1–5 μm (W/(m·K))	5–15 μm (W/(m·K))	15–35 μm (W/(m·K))	35–100 μm (W/(m·K))
200	230	787	1545	2024	2642
250	286	873	1516	1845	2202
300	318	888	1387	1608	1815
350	333	858	1242	1395	1520
400	341	812	1110	1214	1298
450	343	761	992	1069	1131
500	334	708	889	950	998
550	327	658	809	859	886
600	319	619	744	782	814
650	309	587	697	730	753

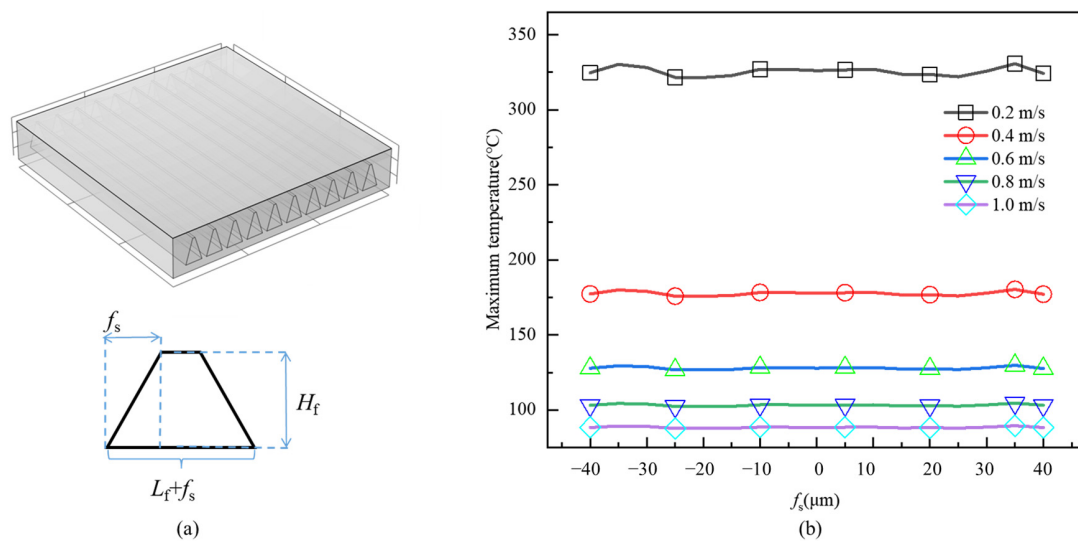**Figure 8.** Heat dissipation performance of diamond microchannels with varying thermal conductivity.

In comparison to the conditions assuming homogeneous thermal conductivity for diamond mentioned earlier, incorporating the effects of thickness and temperature leads to a notable decrease in calculated heat dissipation performance. At a heat flux density of 800 W/(m·K) and an inlet flow rate of 1 m/s, the highest temperature reaches 95.8 °C. This represents a significant decline in heat dissipation performance compared to the scenario with constant diamond thermal conductivity, even falling below that of pure copper. The primary reason for this decline is the lower thermal conductivity of diamond in the 0–1 μm thickness range. Optimizing the growth process during the initial stages of diamond growth or selectively removing the bottom layer of diamond (where growth initiates) without affecting other diamond parts is crucial for enhancing the heat dissipation performance of diamond microchannels.

3.2. Analysis of the Influence of Microchannel Geometry on Heat Dissipation Performance

The impact of microchannel structure on heat dissipation performance is primarily divided into two aspects: (1) the influence of microchannel cross-sectional shape and (2) the influence of overall microchannel geometry. This section investigates how microchannel structure affects the heat dissipation performance of diamond under high-heat-flux-density conditions from these two perspectives.

3.2.1. Research on Influence of Cross-Sectional Shape of Flow Channel on Heat Dissipation Performance

The cross-sectional shape of microchannels significantly influences their heat dissipation capabilities. This section investigates the impact of microchannel shape on the heat dissipation performance of diamond microchannels using a heat source surface heat flux density of 800 W/(m·K), with deionized water as the coolant. To minimize the effects of channel volume changes on heat dissipation, a trapezoidal cross-sectional structure was adopted, where the sum of the upper and lower edges of the trapezoid is $2L_f$, and the height is H_f. The model configuration is depicted in Figure 9a, and the heat dissipation performance under various flow velocity conditions is analyzed in Figure 9b.

Figure 9. Influence of cross-sectional shape on heat dissipation performance: (**a**) schematic of microchannel model and (**b**) impact of cross-sectional variation on heat dissipation performance.

Although the maximum temperature varies with changes in flow velocity, the trend in the maximum temperature variation with f_s remains consistent. The fluctuation range of the highest temperature decreases from around 6 °C to approximately 1 °C with an increasing flow rate. However, compared to the case where $f_s = 0$, varying f_s did not effectively reduce the highest temperature, with the temperature difference being less than 1 °C. It is important to note that as f_s increases, the heat transfer area between the coolant and the diamond substrate gradually increases. This suggests that under high-heat-flux-density and high-coolant-flow-rate conditions, increasing the heat transfer area by altering the microchannel cross-section is not the primary factor influencing the heat dissipation performance of diamond microchannels. Therefore, maintaining a rectangular cross-section ($f_s = 0$) is the optimal choice considering the processing cost of diamond microchannels.

3.2.2. Research on Influence of Channel Geometry on Heat Dissipation Performance

Researchers have extensively investigated diamond-shaped (hourglass-shaped) microchannels [38–40]. Based on this research, this study proposes a multi-diamond-shaped (hourglass-shaped) microchannel structure to explore its heat dissipation performance, aiming to uncover fundamental insights into the effects of diamond-shaped (hourglass-shaped) microchannels on microchannel heat dissipation. To facilitate a more quantitative optimization, this section defines k_1 as the primary parameter controlling the geometric shape of diamond-shaped (hourglass-shaped) microchannels, as shown in Equation (9):

$$k_1 = 2\frac{L_{micro1}}{L_{micro0}} \tag{9}$$

where L_{micro0} denotes the width at the inlet of the channel, as shown in Figure 10a. To ensure a fixed coolant flow rate through the microchannel, L_{micro0} at the inlet remains constant, with $L_f = 120$ μm as previously mentioned above. L_{micro1} represents the channel width at half of the diamond-shaped (hourglass-shaped) microchannel's length in the flow direction. To ensure the model's validity, this study selected k_1 values ranging from 0.3 to 1.5.

(a)

(b)
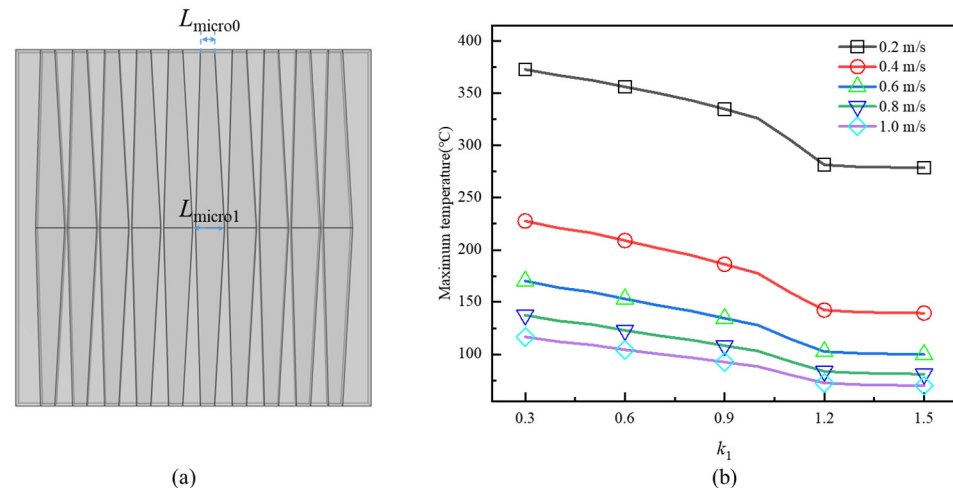
Figure 10. The effect of microchannel expansion on heat dissipation performance: (**a**) microchannel model and (**b**) influence of k_1 on the heat dissipation performance of microchannels.

When $k_1 < 1$, the central region of the microchannel expands, forming an angular microchannel. When $k_1 = 1$, the microchannel model remains consistent with the original configuration. When $k_1 > 1$, the central area of the microchannel contracts, forming an hourglass-shaped microchannel. The calculation results of the heat dissipation effect of diamond microchannels at different flow rates are shown in Figure 10b.

As k_1 increases, the heat dissipation performance of microchannels improves. However, when $k_1 \geq 1.2$, its heat dissipation performance shows little further improvement. For $k_1 < 1.2$, the expansion of microchannels does not significantly increase the heat transfer area but rather increases the maximum temperature of GaN chips. This section examines six typical k_1 values to explore their temperature distributions, as depicted in Figure 11.

(a) $k_1 = 0.3$ (b) $k_1 = 0.5$ (c) $k_1 = 0.7$

(d) $k_1 = 0.9$ (e) $k_1 = 1.1$ (f) $k_1 = 1.3$
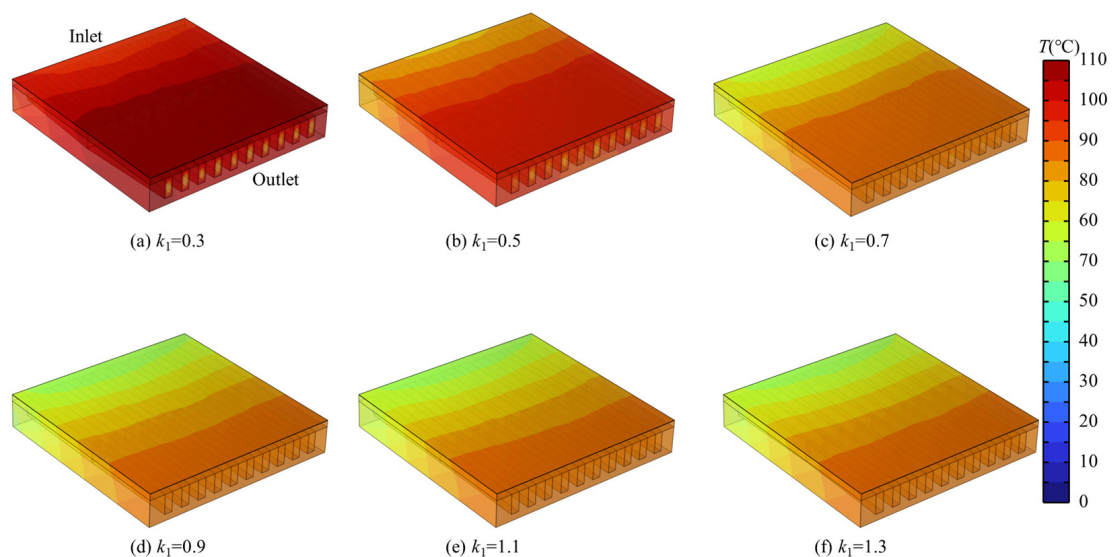
Figure 11. Temperature distribution of microchannels under different k_1 values.

It is evident from Figure 11 that as k_1 increases, the proportion of high-temperature regions decreases while the proportion of low-temperature regions increases, resulting in an overall decrease in temperature across the diamond microchannel. In building upon the earlier analysis of microchannel cross-sectional shape and spacing, it becomes clear that the variation in heat transfer area is not the primary factor influencing heat dissipation performance. This section further examines the impact of flow velocity, with calculation results presented in Figure 12.
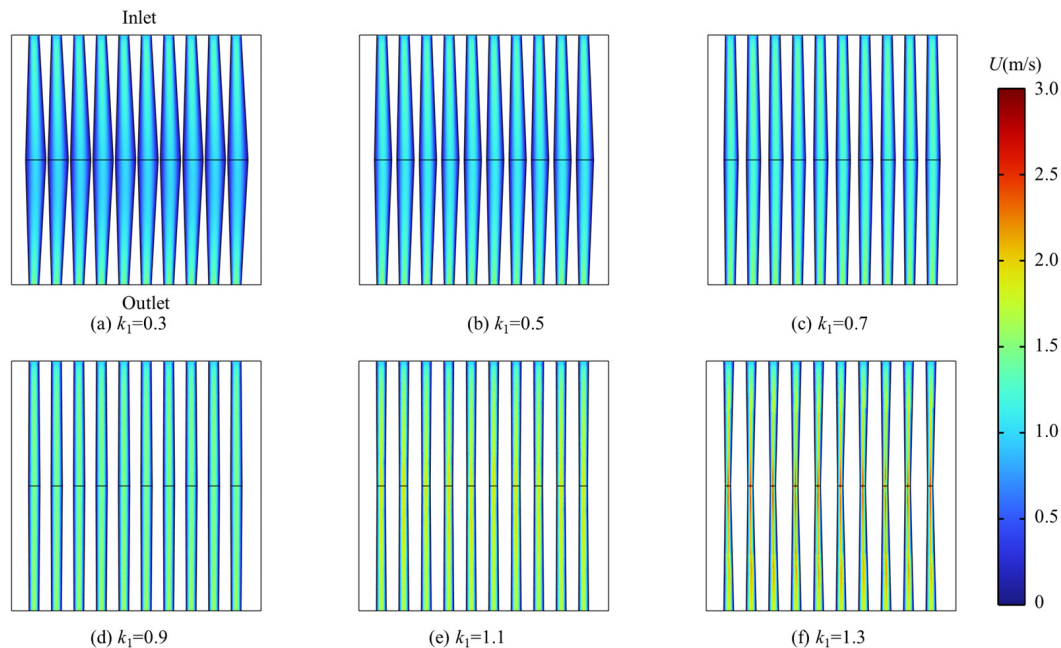

Figure 12. Flow velocity distributions of microchannels under different k_1 values.

According to Figure 12, it is evident that besides the influence of the heat transfer area on temperature distribution, the thickness of the narrow layer in the middle of the microchannel also affects flow velocity. As k_1 increases, multiple regions of high flow velocity appear within the microchannel, enhancing the overall heat transfer capacity of the coolant and improving the microchannel's heat dissipation performance, consequently lowering the maximum temperature of the GaN chip.

Analyzing the pressure distribution, depicted in Figure 13, reveals that as k_1 increases, the maximum water pressure gradually rises, with differences in maximum water pressure under varying conditions spanning an order of magnitude. The higher-pressure region within the microchannels is primarily concentrated near the inlet, primarily due to the narrowing of the middle section of the microchannel.

To investigate the intrinsic relationship between more common microchannel structures and heat dissipation performance, this study explored the impact of multiple diamond-shaped (hourglass-shaped) microchannel units (2,3,4) on the heat dissipation capacity of microchannels. The calculation results are depicted in Figure 14.

It is evident from Figure 14a2–c2 that the highest temperature exhibits a consistent downward trend with the increase in the horizontal axis. However, as k_i (i = 2,3,4) approaches 1.1, the rate of temperature decrease slows down. Specifically, when $k_2 = 1.1$, the maximum temperature decreases by 1.2 °C compared to the standard microchannel $k_2 = 1$. Similarly, for $k_3 = 1.1$, the maximum temperature decreases by 1.7 °C, and for $k_4 = 1.1$, it decreases by 2.4 °C compared to their respective standard microchannel counterparts $k_3 = 1$ and $k_4 = 1$. When k_2, k_3, and $k_4 > 1.1$, the temperature stabilizes (with a maximum temperature difference of less than 0.3 °C under adjacent conditions), and the heat dissipation performance of the microchannel gradually improves with an increase in i (the number of diamond-shaped (hourglass-shaped) units).
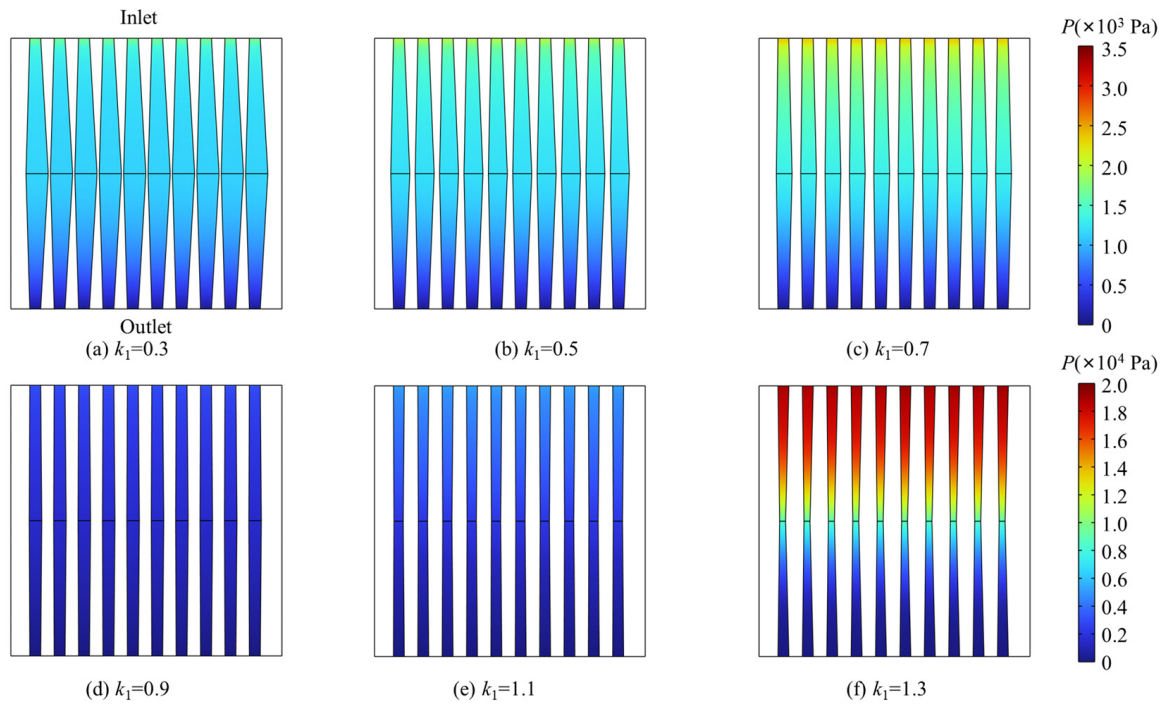
Figure 13. Pressure distribution of microchannels under different k_1 values.
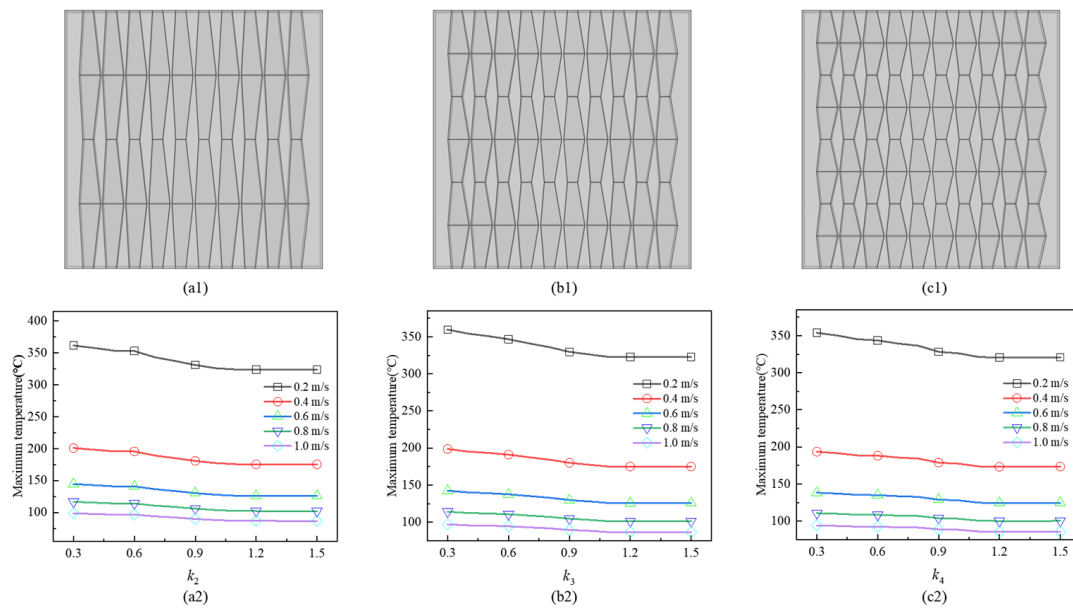
Figure 14. The influence of different numbers of diamond-shaped (hourglass-shaped) microchannels on heat dissipation performance: (**a1**–**c1**) models of diamond-shaped (hourglass-shaped) microchannels with different numbers and (**a2**–**c2**) heat dissipation performance of diamond-shaped (hourglass-shaped) microchannels with different numbers.

Considering that fluid pressure decreases as k_i values increase, it can be concluded that $k_i = 1.1$ offers the best overall heat dissipation performance. This section also analyzes the flow velocity and maximum internal liquid pressure of diamond-shaped (hourglass-shaped) microchannels with different numbers, with calculation results presented in Figure 15.
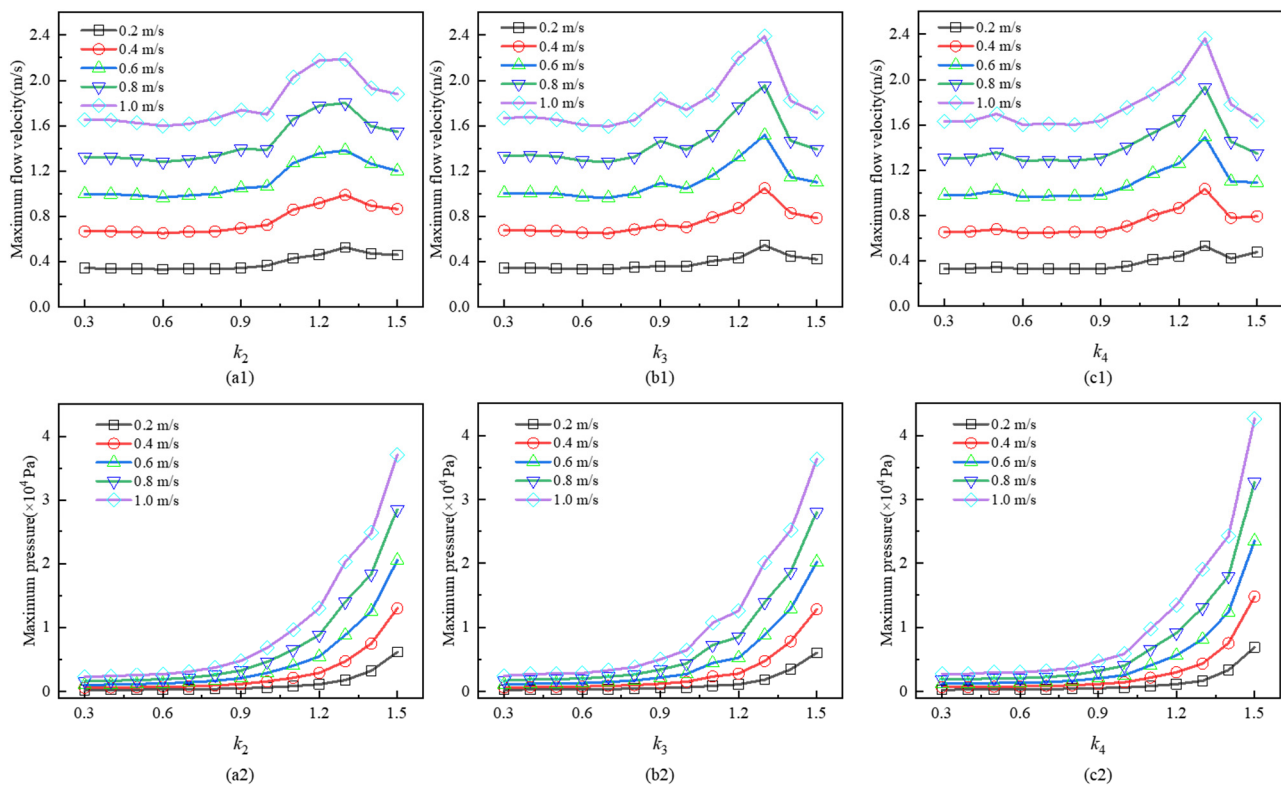
Figure 15. Effects of different numbers of diamond-shaped (hourglass-shaped) microchannels on maximum flow velocity and pressure: (**a1–c1**) effects on flow velocity; (**a2–c2**) effects on maximum pressure.

As i increases, the variations in maximum flow velocity and maximum pressure at $k_i = 1.1$ are relatively minor. This indicates that under identical heat flux density and inlet flow rate conditions, increasing i does not significantly alter the pressure drop but enhances the heat dissipation effectiveness. In conclusion, augmenting the number of diamond-shaped (hourglass-shaped) microchannels is a more effective approach for enhancing the heat dissipation performance of diamond microchannels under consistent conditions.

4. Conclusions

In this study, we modeled diamond microchannels and assessed the validity of our model, investigating the heat dissipation performance under ultra-high-heat-flux-density conditions. The main conclusions drawn are summarized as follows:

(1) Diamond material microchannels exhibit significantly superior heat dissipation effects compared to other common microchannel materials under high-heat-flux-density conditions. The heat dissipation capacity correlates positively with the thermal conductivity of the microchannel materials and shows a linear relationship with the inlet flow velocity. For instance, at a heat flux density of 800 W/cm^2 and inlet flow velocities of 0.4, 0.6, 0.8, and 1 m/s, the highest temperature of diamond microchannels is lower than that of pure copper microchannels by 7.0 °C, 7.2 °C, 7.4 °C, and 7.5 °C, respectively.

(2) The low local thermal conductivity stemming from the growth process of diamond itself is a critical limiting factor for the heat dissipation capacity of microchannels. At a heat flux density of 800 W/(m·K) and an inlet flow rate of 1 m/s, the highest temperature reaches 95.8 °C. The heat dissipation performance of diamond microchannels decreases notably, even falling below that of pure copper. This decline is primarily due to the low thermal conductivity of diamond in the range of 0–1 μm, resulting from the characteristic columnar growth inherent to the MPCVD growth process.

(3) Under the condition of an ultra-high heat flux density of 800 W/cm^2, varying the cross-sectional parameter f_s of the microchannel from 0 to ±40 μm showed minimal

improvement in heat dissipation performance. Compared to the case of $f_s = 0$, changing f_s resulted in a maximum temperature reduction of less than 1 °C. Given the challenges in diamond processing, a rectangular cross-section remains the optimal choice for microchannel fabrication.

(4) Investigating the impact of the number i and shape parameter k_i of diamond-shaped (hourglass-shaped) microchannels on heat dissipation performance revealed that increasing i (the number of diamond-shaped microchannels) led to improved heat dissipation. For instance, at i = 4, the maximum temperature of microchannels decreased by 2.4 °C compared to normal rectangular channel shapes. As ki increased, the maximum temperature of the microchannel gradually decreased. Specifically, at $k_i = 1.1$, the rate of temperature decrease accelerated. Considering the maximum pressure increase in microchannels (especially when k_i exceeds 1.1), it can be concluded that microchannels with $k_i = 1.1$ offer the best comprehensive heat dissipation performance.

These findings provide valuable insights for the design of microchannels in high-power applications. In the future, we will explore the heat dissipation performance of diamond in more complex heat dissipation modes (such as boiling multiphase flow heat dissipation) and further explore the material heat dissipation limit under human ultra-high-heat-flux-density conditions.

Author Contributions: Conceptualization, W.C.; Methodology, J.Z. (Jiwen Zhao) and J.Z. (Jiaqi Zhu); Software, J.Z. (Jiwen Zhao) and K.Z.; Validation, Y.L. and B.D.; Formal analysis, J.Z. (Jiwen Zhao) and X.H.; Data curation, S.Z. and B.L.; Writing—original draft, J.Z. (Jiwen Zhao); Writing—review & editing, J.Z. (Jiwen Zhao). All authors have read and agreed to the published version of the manuscript.

Data Availability Statement: Data are contained within the article.

Conflicts of Interest: Author Xiaobin Hao was employed by the company Henan Core-Diamond Material Technology Co., Ltd. The remaining authors declare that the research was conducted in the absence of any commercial or financial relationships that could be construed as a potential conflict of interest.

Abbreviations

The following abbreviations are used in this manuscript:

Acronym	Meaning
ρ	Density of the diamond substrate or coolant
C_p	Specific heat capacity of the diamond substrate or coolant
Q	Heat source
k	Thermal conductivity of the diamond substrate or coolant
$\mathbf{u}$	Flow velocity of the coolant
p	Pressure of the coolant
$\mathbf{I}$	Second-order unit tensor
$\mathbf{F}$	Volumetric force exerted on the coolant as a whole
$\mathbf{K}$	Viscous stress tensor
μ	Dynamic viscosity of the coolant
$\mathbf{n}_{GaN}/\mathbf{n}_{Dia}$	Normal unit vectors of the contact surface between diamond and GaN
T_{Dia}	Temperature of the diamond layer
T_{GaN}	Temperature of the GaN layer

h_{eq}	Equivalent interfacial thermal conductivity
R_{eq}	Equivalent thermal resistance value
L	Horizontal length
W	Horizontal width
H_1	GaN thickness
H_2	- Grid division basis
L_f	Width of microchannels
δ	Microchannel spacing
H_f	Microchannel height
k_i	Primary parameter controlling the geometric shape of diamond-shaped, i = 1, 2, 3, 4
L_{micro0}	Width at the inlet of the channel
L_{micro1}	Channel width at half of the diamond-shaped (hourglass-shaped) microchannel's length in the flow direction

References

1. Lakshminarayanan, V.; Sriraam, N. The effect of temperature on the reliability of electronic components. In Proceedings of the 2014 IEEE International Conference on Electronics, Computing and Communication Technologies (CONECCT), Bangalore, India, 6–7 January 2014; pp. 1–6.
2. Anandan, S.S.; Ramalingam, V. Thermal management of electronics: A review of literature. *Therm. Sci.* **2008**, *12*, 5–26. [CrossRef]
3. Viswanath, R.; Wakharkar, V.; Watwe, A.; Lebonheur, V. Thermal performance challenges from silicon to systems. *Intel. Technol. J.* **2000**, *4*, 1–16.
4. Deng, Y.; Liu, J. Design of practical liquid metal cooling device for heat dissipation of high performance CPUs. *J. Electron. Packag.* **2010**, *132*, 031009. [CrossRef]
5. Khatibi, M.; Ashrafizadeh, S.N. Mitigating Joule heating in smart nanochannels: Evaluating the efficacy of AC vs. DC fields. *Int. Commun. Heat Mass Transf.* **2024**, *154*, 107448. [CrossRef]
6. Peng, L.; Yu, H.; Chen, C.; He, Q.; Zhang, H.; Zhao, F.; Qin, M.; Feng, Y.; Feng, W. Tailoring dense, orientation–tunable, and interleavedly structured carbon-based heat dissipation plates. *Adv. Sci.* **2023**, *10*, 2205962. [CrossRef]
7. Karimzadeh, M.; Khatibi, M.; Ashrafizadeh, S.N. Impacts of the temperature-dependent properties on ion transport behavior in soft nanochannels. *Int. Commun. Heat Mass Transf.* **2021**, *129*, 105728. [CrossRef]
8. Qin, B.; Zhu, Y.; Zhou, Y.; Qiu, M.; Li, Q. Whole-infrared-band camouflage with dual-band radiative heat dissipation. *Light Sci. Appl.* **2023**, *12*, 246. [CrossRef]
9. Liu, Y.; Xu, Z.; Wu, J.; Wei, D.; Guan, X. Coordinated Optimization for Energy Efficient Thermal Management of 5G Base Station Site. *IFAC-Pap.* **2022**, *55*, 102–107. [CrossRef]
10. Sun, M.; Zhao, X.; Tan, H.; Li, X. Coordinated operation of the integrated electricity-water distribution system and water-cooled 5G base stations. *Energy* **2022**, *238*, 122034. [CrossRef]
11. Gao, X.; Han, X.; Zhao, Z.; Huang, N.-Y.; Jiao, K.; Song, P.; Zhu, J.; Wang, Y. Lewis functional nanodiamonds for efficient metal-free photocatalytic CO_2 reduction. *J. Mater. Chem. A* **2024**. [CrossRef]
12. Zhao, X.; Su, L.; Jiang, J.; Deng, W.; Zhao, D. A review of working fluids and flow state effects on thermal performance of micro-channel oscillating heat pipe for aerospace heat dissipation. *Aerospace* **2023**, *10*, 179. [CrossRef]
13. Gao, X.-W.; Zhao, Z.-W.; He, Y.; Fan, S.-F.; Jiao, K.-R.; Lou, S.-Y.; Han, X.-Y.; Song, P.-F.; Cai, R.; Hu, Z. Nanodiamond: A promising metal-free nanoscale material in photocatalysis and electrocatalysis. *Rare Met.* **2024**, *43*, 3501–3552. [CrossRef]
14. *COMSOL Multiphysics®*, Version 6.2; COMSOL Multiphysics: Stockholm, Sweden, 2024.
15. Tuckerman, D.B.; Pease, R.F.W. High-performance heat sinking for VLSI. *IEEE Electron Device Lett.* **1981**, *2*, 126–129. [CrossRef]
16. Qu, G.; Deng, Z.; Guo, W.; Peng, Z.; Jia, Q.; Deng, E.; Zhang, H. The heat-dissipation sintered interface of power chip and heat sink and its high-temperature thermal analysis. *IEEE Trans. Compon. Packag. Manuf. Technol.* **2023**, *13*, 816–822. [CrossRef]
17. He, Z.; Yan, Y.; Zhang, Z. Thermal management and temperature uniformity enhancement of electronic devices by micro heat sinks: A review. *Energy* **2021**, *216*, 119223. [CrossRef]
18. Kidalov, S.V.; Shakhov, F.M. Thermal conductivity of diamond composites. *Materials* **2009**, *2*, 2467–2495. [CrossRef]
19. Graebner, J.E. Thermal conductivity of diamond. In *Diamond: Electronic Properties and Applications*; Springer: New York, NY, USA, 1995; pp. 285–318.
20. Qi, Z.; Zheng, Y.; Wei, J.; Yu, X.; Jia, X.; Liu, J.; Chen, L.; Miao, J.; Li, C. Surface treatment of an applied novel all-diamond microchannel heat sink for heat transfer performance enhancement. *Appl. Therm. Eng.* **2020**, *177*, 115489. [CrossRef]
21. Li, W.; Zhu, L.; Ji, F.; Yu, J.; Jin, Y.; Wang, W. Multi-Parameters Optimization for Diamond Microchannel Heat Sink. In Proceedings of the 2019 20th International Conference on Electronic Packaging Technology (ICEPT), Hong Kong, China, 12–15 August 2019; pp. 1–4. [CrossRef]
22. Yang, Q.; Zhao, J.; Huang, Y.; Zhu, X.; Fu, W.; Li, C.; Miao, J. A diamond made microchannel heat sink for high-density heat flux dissipation. *Appl. Therm. Eng.* **2019**, *158*, 113804. [CrossRef]
23. Junlei, T.; Jiadong, S.; Liangxian, C.; Jinlong, L.; Chengming, L.; Junjun, W. Surface termination of the diamond microchannel and single-phase heat transfer performance. *Int. J. Heat Mass Transf.* **2022**, *199*, 123481. [CrossRef]

24. Sarma, P.; Patowari, P.K. A Review on Fluid Flow and Mixing in Microchannel and their Design and Manufacture for Microfluidic Applications. *Micro Nanosyst.* **2023**, *15*, 167–184. [CrossRef]

25. Xiang, J.; Deng, L.; Zhou, C.; Zhao, H.; Huang, J.; Tao, S. Heat transfer performance and structural optimization of a novel micro-channel heat sink. *Chin. J. Mech. Eng.* **2022**, *35*, 38. [CrossRef]

26. Xia, G.; Jiang, J.; Wang, J.; Zhai, Y.; Ma, D. Effects of different geometric structures on fluid flow and heat transfer performance in microchannel heat sinks. *Int. J. Heat Mass Transf.* **2015**, *80*, 439–447. [CrossRef]

27. Rajalingam, A.; Chakraborty, S. Effect of shape and arrangement of micro-structures in a microchannel heat sink on the thermohydraulic performance. *Appl. Therm. Eng.* **2021**, *190*, 116755. [CrossRef]

28. Deng, D.; Pi, G.; Zhang, W.; Wang, P.; Fu, T. Numerical Study of Double-Layered Microchannel Heat Sinks with Different Cross-Sectional Shapes. *Entropy* **2018**, *21*, 16. [CrossRef] [PubMed]

29. Ahmad, F.; Ahmed, F.; Ali, H.; Rehman, Z.; Suleman, M.; Raouf, I. Effect of Cross-Sectional Geometry on Hydrothermal Behavior of Microchannel Heat Sink. *J. Non-Equilib. Thermodyn.* **2022**, *47*, 269–287. [CrossRef]

30. Jing, D.; He, L. Numerical studies on the hydraulic and thermal performances of microchannels with different cross-sectional shapes. *Int. J. Heat Mass Transf.* **2019**, *143*, 118604. [CrossRef]

31. Parlak, Z. Optimal design of wavy microchannel and comparison of heat transfer characteristics with zigzag and straight geometries. *Heat Mass Transf.* **2018**, *54*, 3317–3328. [CrossRef]

32. Dai, Z.; Fletcher, D.F.; Haynes, B.S. Impact of tortuous geometry on laminar flow heat transfer in microchannels. *Int. J. Heat Mass Transf.* **2015**, *83*, 382–398. [CrossRef]

33. Fedorov, A.G.; Viskanta, R. Three-dimensional conjugate heat transfer in the microchannel heat sink for electronic packaging. *Int. J. Heat Mass Transf.* **2000**, *43*, 399–415. [CrossRef]

34. Cho, J.; Li, Z.; Bozorg-Grayeli, E.; Kodama, T.; Francis, D.; Ejeckam, F.; Faili, F.; Asheghi, M.; Goodson, K.E. Improved thermal interfaces of GaN–diamond composite substrates for HEMT applications. *IEEE Trans. Compon. Packag. Manuf. Technol.* **2012**, *3*, 79–85. [CrossRef]

35. Cho, J.; Francis, D.; Altman, D.H.; Asheghi, M.; Goodson, K.E. Phonon conduction in GaN-diamond composite substrates. *J. Appl. Phys.* **2017**, *121*, 055105. [CrossRef]

36. Zhou, Y.; Anaya, J.; Pomeroy, J.; Sun, H.; Gu, X.; Xie, A.; Beam, E.; Becker, M.; Grotjohn, T.A.; Lee, C. Barrier-layer optimization for enhanced GaN-on-diamond device cooling. *ACS Appl. Mater. Interfaces* **2017**, *9*, 34416–34422. [CrossRef] [PubMed]

37. Song, C.; Kim, J.; Cho, J. The effect of GaN epilayer thickness on the near-junction thermal resistance of GaN-on-diamond devices. *Int. J. Heat Mass Transf.* **2020**, *158*, 119992. [CrossRef]

38. Goli, S.; Saha, S.K.; Agrawal, A. Hydrothermal and Second Law Analyses of Fluid Flow in Converging-Diverging (Hourglass) Microchannel. *Heat Transf. Eng.* **2023**, *44*, 277–302. [CrossRef]

39. Goli, S.; Saha, S.K.; Agrawal, A. Thermo-fluidic behaviour of diamond and hourglass microchannels: Investigation from the second law viewpoint. *Int. J. Heat Mass Transf.* **2023**, *205*, 123886. [CrossRef]

40. Goli, S.; Saha, S.K.; Agrawal, A. Study of hydrothermal transport phenomena and performance characteristics for a flow through a diamond (diverging-converging) microchannel. *Therm. Sci. Eng. Prog.* **2022**, *29*, 101195. [CrossRef]